PHYSICAL REVIEW B VOLUME 51, NUMBER 20 15 MAY 1995-II

Electronic structure of $La_{1-x}Sr_xMnO_3$ studied by photoemission and x-ray-absorption spectroscopy

T. Saitoh, A. E. Bocquet, T. Mizokawa, H. Namatame,* and A. Fujimori
Department of Physics, University of Tokyo, Bunkyo-ku, Tokyo 113, Japan

M. Abbate
Laboratorio Nacional de Luz Sincrotron, Caixa Postal 6192, Campinas, 13081-970, Brazil

Y. Takeda
Department of Chemistry, Faculty of Engineering, Mie University, Tsu 514, Japan

M. Takano
Institute for Chemical Research, Kyoto University, Uji, Kyoto 611, Japan

(Received 25 January 1995)

The electronic structure of $La_{1-x}Sr_xMnO_3$ has been studied by photoemission and O 1s x-ray-absorption spectroscopy. Spectra of the Mn 2p core levels and the valence bands for $LaMnO_3$ and $SrMnO_3$ have been analyzed using a configuration-interaction cluster model. The ground state of $LaMnO_3$ is found to be mixed d^4 and $d^5\underline{L}$ states and that of $SrMnO_3$ to be heavily mixed d^3 and $d^4\underline{L}$ states, reflecting their strong covalency. The character of the band gap of $LaMnO_3$ is of the p-to-d charge-transfer type while that of $SrMnO_3$ has considerable p-p character as well as p-d character. Holes doped into $LaMnO_3$ mainly of oxygen p character are coupled antiferromagnetically with the d^4 local moments of the Mn^{3+} ions and become itinerant, thus aligning the Mn moments ferromagnetically. The changes in the electronic structure with carrier doping are not of the rigid band type: By La substitution for $SrMnO_3$, the so-called in-gap spectral weight (of $e_{g\uparrow}$ symmetry) appears with its peak located 1–2 eV below the Fermi level and grows in intensity with increasing La concentration, while the spectral intensity of the $e_{g\uparrow}$ states above the Fermi level decreases, showing a transfer of spectral weight from the unoccupied to the occupied $e_{g\uparrow}$ states with electron doping. Meanwhile, the intensity at the Fermi level remains low even in the metallic phase ($0.2 \lesssim x \lesssim 0.6$). The energy shifts of core-level peaks and valence-band features with x suggest a downward shift of the Fermi level with hole doping, but the shift is found to be very small in the metallic phase. The importance of the orbital degeneracy of the $e_{g\uparrow}$ band and possible orbital fluctuations in the ferromagnetic phase are pointed out.

I. INTRODUCTION

Since the discovery of high-temperature superconductivity in doped Cu oxides,[1] interest has been revived in 3d transition-metal (TM) oxides. Many 3d TM oxides, including high-T_c Cu oxides, show metallic conductivity when doped with a sufficient amount of extra holes or electrons. Since high-T_c superconductivity appears in the vicinity of doping-induced insulator-to-metal transitions, understanding the nature of the insulator-to-metal transitions and the resulting metallic states in various 3d TM oxides will provide important knowledge to understand the high-T_c Cu oxides. Photoemission spectroscopy is a powerful tool to investigate the electronic structures of 3d TM oxides[2,3] and their changes with carrier doping. Carrier doping in charge-transfer-type $La_{2-x}Sr_xNiO_4$ (Ref. 4) and Mott-Hubbard-type $La_xSr_{1-x}TiO_3$ (Ref. 5) has been studied by photoemission spectroscopy. It has been found that hole doping (Sr substitution) in $La_{2-x}Sr_xNiO_4$ induces spectral weight above the Fermi level within the band gap of La_2NiO_4, and that the Fermi level is located near the top of the valence band. As for $La_xSr_{1-x}TiO_3$, electron doping (La substitution) induces spectra weight of Ti 3d character below the Fermi level within the band gap of $SrTiO_3$, and the Fermi level is located near the bottom of the conduction band. In either case, the doping-induced spectral weight is distributed over a wide energy range of a few eV so that it fills the band gap of the parent insulator. It is therefore of great interest to see whether such a highly non-rigid-band-like behavior is a common feature of carrier doping in 3d TM oxides, and how it is related to insulator-to-metal transitions and the appearance of superconductivity in Cu oxides.

In the present work, we investigated a perovskite-type system $La_{1-x}Sr_xMnO_3$, which is intermediate between typical Mott-Hubbard-type (Ti and V) compounds[6] and charge-transfer-type (Cu and Ni) compounds. In this system, the valence of the Mn ion can be controlled from 3+ ($LaMnO_3$) to 4+ ($SrMnO_3$), and therefore the system can be viewed either as a hole-doped $LaMnO_3$ or an electron-doped $SrMnO_3$. Unlike the Ti, Ni, and Cu compounds, the magnitude of the spin is large ($S=2-5/2$) in the Mn and Fe compounds: The end members $LaMnO_3$ and $SrMnO_3$ are antiferromagnetic insulators, while the system becomes a ferromagnetic metal in the intermedi-

0163-1829/95/51(20)/13942(10)/$06.00

ate composition range $0.2 < x < 0.6$. The earliest survey of this system was done by Jonker and van Santen,[7,8] and several works followed it. $LaMnO_3$ has a orthorhombically or monoclinically distorted perovskite structure[9–13], while $SrMnO_3$ has a cubic perovskite structure.[14] $LaMnO_3$ is an *A*-type antiferromagnet,[10,12] in which ferromagnetic (001) layers with alternating spin directions are stacked along the *c* axis. The *A*-type antiferromagnetism is accompanied by a Jahn-Teller distortion of the Mn^{3+} ion with $3d^4$ configuration. A Néel temperature T_N of 100–141 K (Refs. 10 and 12) has been reported. $SrMnO_3$ is a *G*-type antiferromagnet with $T_N = 260$ K,[15] in which all the nearest-neighbor Mn ions have opposite spins. Magnetic and electrical measurements have revealed that for $0.2 < x < 0.6$, the system shows metallic conductivity below the Curie temperature.[8,16] Zener[17] and subsequently de Gennes[18] explained it by the so-called double-exchange mechanism. Recently giant negative magnetoresistance has been reported for $La_{1-x}Sr_xMnO_3$,[19] indicating a strong coupling between ferromagnetism and metallic conductivity in this system.

In this paper, we present results of photoemission and x-ray-absorption (XAS) studies on $La_{1-x}Sr_xMnO_3$. In order to characterize the electronic structure of the end members $LaMnO_3$ and $SrMnO_3$, a configuration-interaction (CI) cluster-model analysis was made of the Mn $2p$ core-level, valence-band, and O $1s$ XAS spectra. The doping dependence of the electronic structure is also studied, with a particular emphasis on the appearance of in-gap spectral weight and the shift of the Fermi level with carrier doping.

II. EXPERIMENTAL

Polycrystalline samples of $La_{1-x}Sr_xMnO_3$ were prepared by solid-state reaction. Sintered mixtures of appropriate molar quantities of La_2O_3, $SrCO_3$, and Mn_2O_3 were pressed into pellets and prefired in air at 1000 °C for 12 h. Ground again, well mixed, and pressed into pellets, they are fired on a platinum foil at 1300 °C for 48 h in air. Subsequent processing for each sample was carried out as follows. For $LaMnO_3$, the pellet was fired again at 1300 °C in air and quenched into liquid N_2. For $La_{0.9}Sr_{0.1}MnO_3$ and $SrMnO_3$, the pellets were fired at 1500 °C for 3 h in air, quenched into liquid N_2, and then annealed in an O_2 atmosphere at 300 °C for 24 h. As for $La_{0.9}Sr_{0.1}MnO_3$, the pellet was further fired at 1300 °C for 6 h in air and quenched into liquid N_2. Pellets from $x = 0.3–0.7$ were fired at 1000 °C for 24 h in an O_2 gas flow and slowly cooled to room temperature. As for $La_{0.1}Sr_{0.9}MnO_3$ and $SrMnO_3$, the pellets were further fired at 1300 °C for 24 h in N_2 gas flow and quenched into liquid N_2.

X-ray photoemission spectroscopy (XPS) and ultraviolet photoemission spectroscopy (UPS) measurements were carried out using a spectrometer equipped with a Mg $K\alpha$ source ($h\nu = 1253.6$ eV), an He discharge lamp (He I: $h\nu = 21.2$ eV, He II: $h\nu = 40.8$ eV) and a Physical Electronics double-pass cylindrical mirror analyzer. The XPS spectra were corrected for the Mg $K\alpha_{3,4}$ ghost. The total-energy resolution was about 1.0, 0.35, and 0.25 eV for XPS, He II UPS, and He I UPS, respectively. UPS spectra including $3p$-$3d$ resonant-photoemission spectra were also measured at beamline BL-2 of the Synchrotron Radiation Laboratory (SRL), Institute for Solid State Physics, University of Tokyo. In order to obtain fresh, clean surfaces, the samples were scraped with a diamond file in the spectrometer chamber at liquid-nitrogen temperatures (~80 K). In the case of XPS, the scraping was made until the O $1s$ core-level spectrum became a single peak and did not change with further scrapings. As shown in Fig. 1, the filing was successful for almost all samples in reducing the intensity of a shoulder or tail on the higher binding-energy side of the O $1s$ peak, which is usually associated with contaminants on, or degradation of, the surface. In the case of UPS, the scraping was made until a bump around 9–10 eV disappeared, and the whole spectrum did not change with further scrapings. We paid attention to the intensity of this bump and a structure around 5–6 eV, which increased with time due to degradation of the surface. We estimated the degradation time of the surfaces by observing the change of the O $1s$ spectrum and the valence-band spectrum for XPS and UPS, respectively, and scraped the samples before the degradation. The degradation time was typically 1–2 h for XPS and the measurements at SRL, and less than 1 h for UPS using the He lamp. All the spectra were recorded at liquid-nitrogen temperatures (~80 K) to prevent the removal of oxygen from the surface under ultrahigh-vacuum conditions. The base pressure in the spectrometer was in the low 10^{-10}-Torr range for all the measurements. The Fermi edges of all measurements were calibrated using the Au Fermi edge and, for the XPS spectra, the Au $4f_{7/2}$ (84.0 eV) and Cu $2p_{3/2}$ (932.6 eV) core levels were also used for the calibration of the binding energies. XAS measurements were done at Berliner Elektronen Speicherring-Gesellschaft für Synchrotron-

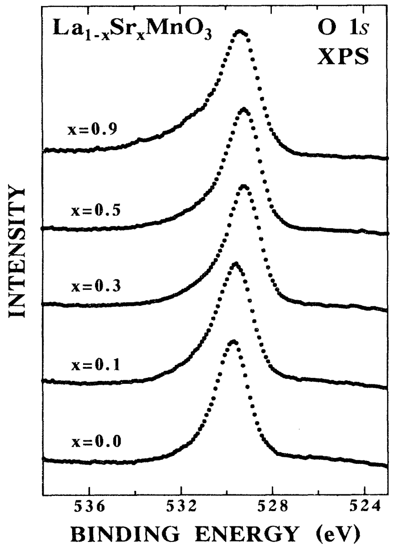

FIG. 1. O $1s$ core-level XPS spectra of $La_{1-x}Sr_xMnO_3$.

strahlung (BESSY) in Berlin: The photon energies have been calibrated using the O 1*s* absorption peak of TiO_2 at 530.7 eV. Details are described in Ref. 20.

III. ELECTRONIC STRUCTURE OF $LaMnO_3$ AND $SrMnO_3$

A. Configuration-interaction cluster model

In order to determine the electronic structures of the end members of the present system, we performed CI cluster-model calculations for the Mn 2*p* core-level, valence-band, and O 1*s* XAS spectra of $LaMnO_3$ and $SrMnO_3$. (We compare calculations for $SrMnO_3$ with measured spectra of $La_{0.1}Sr_{0.9}MnO_3$, assuming that the difference is small between these two compositions.) We consider that the octahedral clusters $[Mn^{3+}(O^{2-})_6]^{-9}$ and $[Mn^{4+}(O^{2-})_6]^{-8}$ are good starting points to study the electronic structure of $LaMn^{3+}O_3$ and $SrMn^{4+}O_3$, respectively, because we believe that electron-electron interaction and *p*-*d* hybridization within the cluster dominate interactions between the clusters. In the present cluster-model calculations, we neglected the off-diagonal matrix elements of the Coulomb interaction and retained only the diagonal part of the *d*-*d* Coulomb and exchange interaction. On the other hand, we have included the anisotropy in the metal-ligand hybridization[21,22] which were not included in previous CI cluster-model analyses.[23]

The present model has three adjustable parameters, namely the *d*-*d* Coulomb interaction U, the ligand *p*-to-TM *d* charge-transfer energy Δ, and the ligand *p*-TM *d* transfer integral $(pd\sigma)$. It should be noted that U is defined with respect to the centers of gravity of the d^{n-1}, d^n and d^{n+1} configurations, and Δ with respect to the centers of gravity of the d^n and $d^{n+1}\underline{L}$ configurations, where $\underline{L}$ denotes a ligand hole. We use Kanamori parameters,[24] u, u', and j, which are given in terms of Racah parameters A, B, and C.[25] We have fixed the values of B and C to those of the free ions[26] as shown in Table I. The method of the core-level calculations is the same as in previous calculations,[21,22] and that of the valence-band calculations is essentially the same as that in Ref. 2 except that the present calculations do not include off-diagonal Coulomb matrix elements. In the calculations of the O 1*s* XAS spectra, we have neglected interaction between the O 1*s* core hole and the valence electrons, for simplicity. Details are given in Refs. 2, 21, and 22.

We have also calculated physical quantities, such as the band gaps, the net *d*-electron numbers, and the character of doped carriers within the CI cluster model. We define by U_{eff} and Δ_{eff}, respectively, the *d*-*d* Coulomb energy and the charge-transfer energy with respect to the lowest energies of the multiplets. U and Δ represent the smooth variation of the electronic structure of the TM compounds as a function of the TM atomic number and valence,[21] while the actual physical properties are more directly related to U_{eff} and Δ_{eff},[22] which contain the nonmonotonic variation of the multiplet splitting.

The *d* component of a doped hole and that of a doped electron are given by $N_d(n)-N_d(n-1)$ and $N_d(n+1)-N_d(n)$, respectively, where $N_d(n)$ is the net *d*-electron numbers of the ground state with nominal *d*-electron number n. The final states of valence-band photoemission and inverse photoemission that are closest to the Fermi level are considered to be the ground states of the hole-doped and electron-doped systems, respectively. We may then define the *d* character of the doped hole and electron as

$$C^d_{\text{hole}} \equiv N_d(n)-N_d(n-1) \tag{1}$$

and

$$C^d_{\text{electron}} \equiv N_d(n+1)-N_d(n) \; , \tag{2}$$

respectively. We can also define the *p* character of the doped hole and electron as $C^p_{\text{hole}} \equiv 1-C^d_{\text{hole}}$ and $C^p_{\text{hole}} \equiv 1-C^d_{\text{electron}}$, respectively. By this definition, $0 \le C^d_{\text{hole}}$ and $C^d_{\text{electron}} \le 1$; doped carriers are *d*-like for $C^d_{\text{hole}} > 0.5$ or $C^d_{\text{electron}} > 0.5$ and *p* like for $C^d_{\text{hole}} < 0.5$ or $C^d_{\text{electron}} < 0.5$.

B. Photoemission spectra and the results of cluster-model analyses

In the calculations of the spectra, we varied the parameters U, Δ, and $(pd\sigma)$ so that we could obtain the best fit to the experimental data of the Mn 2*p* core-level, valence-band, and O 1*s* XAS spectra using a single set of parameters. We have assumed a high-spin state in our calculations. It will be shown below (Sec. IV A) that the Mn *d* electrons in $LaMnO_3$ are indeed in the high-spin state.

In Fig. 2, the Mn 2*p* core-level spectra are shown. All the spectra display $2p_{3/2}$ and $2p_{1/2}$ spin-obit doublet peaks located at ~642 and ~654 eV, respectively. Since we used a Mg $K\alpha$ source, emission due to the Mn *LMV* Auger peak is observed on the higher binding-energy side of the $2p_{1/2}$ peak. This Auger peak partially obscures the $2p_{1/2}$ satellite structure, while the satellite is clearly observed in the spectra taken with an Al $K\alpha$ light source by Lam and Veal.[27] In the latter spectra, the satellite is located at binding energies about 11 eV higher than the main peak. This means that the satellite accompanying the Mn $2p_{3/2}$ peak overlaps the Mn $2p_{1/2}$ main peak. Indeed, the satellite structure was clearly observed in the Mn 3*p* peak as well.

The calculated Mn 2*p* spectra for $LaMnO_3$ and $SrMnO_3$ are compared with experiment in Figs. 3(a) and 3(b), respectively. The calculated spectra have been broadened with a Lorentzian function whose width is en-

TABLE I. Values for parameters obtained from the CI cluster-model analyses of the Mn 2*p* core-level photoemission spectra (in eV). Errors are ±0.5 eV for Δ and U and ±0.1 eV for $(pd\sigma)$. Racah B and C parameters used in the analysis are also shown (in eV).

	B	C	Δ	U	$(pd\sigma)$	Δ_{eff}	U_{eff}
$LaMnO_3$	0.120	0.552	4.5	7.8	−1.8	1.8	6.8
$SrMnO_3$	0.132	0.610	2.0	7.5	−1.5	−0.2	7.1

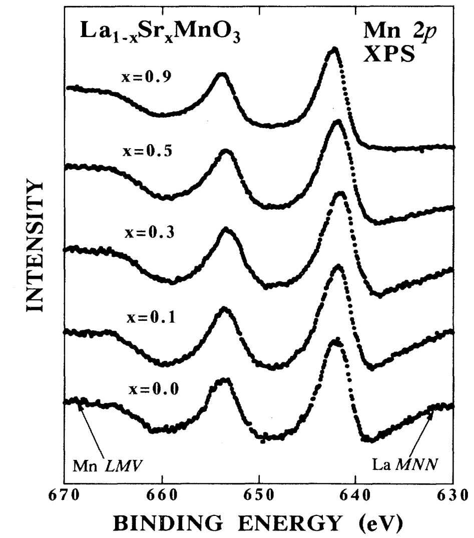

FIG. 2. Mn 2p core-level XPS spectra of $La_{1-x}Sr_xMnO_3$.

ergy dependent, and a Gaussian function.[28] Good agreement with experiment was obtained for parameters listed in Table I. For $LaMnO_3$, the main peaks arise largely from $2\underline{p}d^5\underline{L}$ states, whereas the satellites are due to $2\underline{p}d^4$ and $2\underline{p}d^6\underline{L}^2$ states. In the case of $SrMnO_3$, good agreement with experiment was obtained for smaller Δ (see Table I); the main peak has heavily mixed $2\underline{p}d^4\underline{L}-2\underline{p}d^5\underline{L}^2$ character, while the satellite structure is primarily due to $2\underline{p}d^5\underline{L}^2$ states.

One can see from Table I that for both $LaMnO_3$ and $SrMnO_3$, $U>\Delta$ and $U_{\mathrm{eff}}>\Delta_{\mathrm{eff}}$, which means that these compounds are charge-transfer-type insulators. It has been thought that Mn oxides are intermediate between the typical Mott-Hubbard-type compounds (such as Ti oxides) and charge-transfer-type compounds (such as Cu and Ni oxides). In the present case, Δ's are small due to the high valences of Mn, and therefore the compounds are located in the charge-transfer regime. It is noted, however, that the Δ_{eff} or $SrMnO_3$ is nearly 0 eV, and hence the band gap will have considerable p-p character[29] in addition to the p-d character. The calculated band gaps E_{gap}, the net d-electron numbers N_d, and the character of doped carriers for $LaMnO_3$ and $SrMnO_3$ are listed in Table II. The band gap of $SrMnO_3$ is a little larger than that of $LaMnO_3$, which may be related to the experimental fact that the metallic range is located closer to the $LaMnO_3$ end rather than the $SrMnO_3$ end. The N_d's of both systems, especially that of $SrMnO_3$, considerably deviate from the nominal values (4 for $LaMnO_3$ and 3 for $SrMnO_3$), indicating that their ground states are strongly hybridized. The ground state of $LaMnO_3$ consists of $\sim 50\%$ d^4, $\sim 40\%$ $d^5\underline{L}$, and $\sim 10\%$ $d^6\underline{L}^2$ states, and the ground state of $SrMnO_3$ consists of $\sim 40\%$ d^3, $\sim 50\%$ $d^4\underline{L}$, and $\sim 10\%$ $d^5\underline{L}^2$ states. Table II shows that doped holes in $LaMnO_3$ have predominant p character, while

TABLE II. Band gaps (E_{ggap}), net d-electron numbers (N_d), and d characters of doped carriers (C^d_{hole} and C^d_{electron}).

	E_{gap} (eV)	N_d	C^d_{hole}	C^d_{electron}
$LaMnO_3$	1.7	4.5	0.23	
$SrMnO_3$	2.3	3.8		0.43

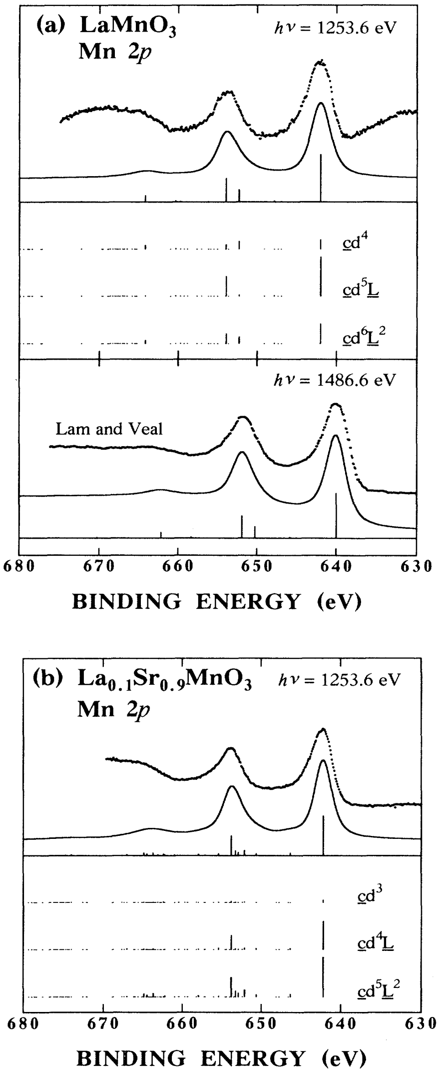

FIG. 3. Cluster-model analyses of the Mn 2p core-level spectra of $LaMnO_3$ (a) and $La_{0.1}Sr_{0.9}MnO_3$ (b). Upper panels: Calculated Mn 2p spectra (solid lines) are compared with the experimental spectra (dots). Lower panels: Decomposition of the line spectra into final-state configurations. For $LaMnO_3$, the calculated spectrum (solid line) is also compared with the experimental spectrum by Lam and Veal (Ref. 27) (dots) which was taken with an Al $K\alpha$ source and therefore shows no Mn LMV Auger peak.

doped electrons in $SrMnO_3$ have both *p* and *d* character to a comparable extent.

Recently, Chainani, Mathew, and Sarma[13] analyzed the Mn 2*p* core-level photoemission spectrum of $LaMnO_3$ using the cluster model, and obtained $\Delta=5.0$ eV, $U=4.0$ eV, and $(pd\sigma)=-2.2$ eV. From this result, they suggested that $LaMnO_3$ is more Mott-Hubbard-like than charge-transfer-like. We consider that the disagreement between their parameter values and ours comes mainly from the following reasons: They have not considered the difference between u and u', and assumed $10Dq=1.0$ eV, and fixed the energy difference between oxygen t_{2g} and e_g states at 1.5 eV. $10Dq$ is not considered in our model. They have taken the *d*-*d* exchange coupling to be 0.5 eV, while our value is 0.85 eV for $LaMnO_3$. They fixed the value of U which they obtained from the comparison of the Mn $L_{23}M_{45}M_{45}$ Auger spectrum with the self-convolution of the Mn 3*d* partial DOS. We think that the latter method of estimating U would need further theoretical justification. Also, the definition of Δ is a little different. Nevertheless, it is interesting to note that their ground-state components of $LaMnO_3$ (50% d^4, 41% $d^5\underline{L}$, and 9% $d^6\underline{L}^2$ states) are very close to ours in spite of the different parameter sets. Whatever the parameter values, both results indicate a heavily mixed ground state.

In Figs. 4(a) and 4(b), using the cluster model we reproduced the experimental data for $h\nu=100$ eV, which includes emission from the O 2*s* and La 5*p* or Sr 4*p* core levels. Note that, in order to simulate the O 2*p* band, we used the He I spectra, whose intensity is mostly due to O 2*p* states.[30] Here the Mn 3*d*-to-O 2*p* ratio was fixed to the calculated photoionization cross section[30] (including the empirical multiplication factor of ~3 for the O 2*p* states[31]). The O 1*s* XAS spectra[20] are compared with the ligand O 2*p* component of the unoccupied states of the calculated spectra. The calculated spectra are broadened with Lorentzian and Gaussian functions to represent the lifetime and instrumental broadening. For the Lorentzian broadening, an additional energy-dependent broadening as employed in the Mn 2*p* core-level analysis is also assumed.[32] The experimental O 1*s* XAS spectra are referenced to the O 1*s* XPS binding energies. In this way, the first peak in the XAS spectra is located ~0.3 eV above the Fermi level.[33] The energy scale of the calculated valence-band spectrum of $LaMnO_3$ has been chose so that the first ionization state ($e_{g\uparrow}$ state) coincides with the peak in the experimental $LaMnO_3-La_{0.1}Sr_{0.9}MnO_3$ difference spectrum (see Fig. 11). The energy gap between the calculated valence-band and O 1*s* XAS spectra is set equal to the calculated band gap. For $SrMnO_3$, the energy scale of the calculated spectrum has been chose so that the first occupied $t_{2g\uparrow}$ states are located closer to the Fermi level by ~0.8 eV than those in $LaMnO_3$, considering the energy shifts of various features between $LaMnO_3$ and $SrMnO_3$ (see Sec. IV).

Figures 4(a) and 4(b) show that the calculated spectra have satellite structures 12–15 eV below the Fermi level. Such satellites can indeed be identified in the 3*p*-3*d* resonant-photoemission spectra as shown in Fig. 5, where enhancement is observed at 10–15 eV in the on-resonance spectra. The apparent decrease in intensity in the region 1–7 eV in going from off-resonance to on-resonance spectra is due to the rapid decrease of the photoionization cross section of the O 2*p* states with photon energy.[30]

Figure 4(a) shows that for the valence band of $LaMnO_3$ the main band located at 1–7 eV below the Fermi level will have mainly $d^4\underline{L}$ character, while the satellite structure located at 12–14 has heavily mixed d^3-$d^5\underline{L}^2$ character. The structure close to the Fermi level is due to emission from the $e_{g\uparrow}$ states and the second structure is due to

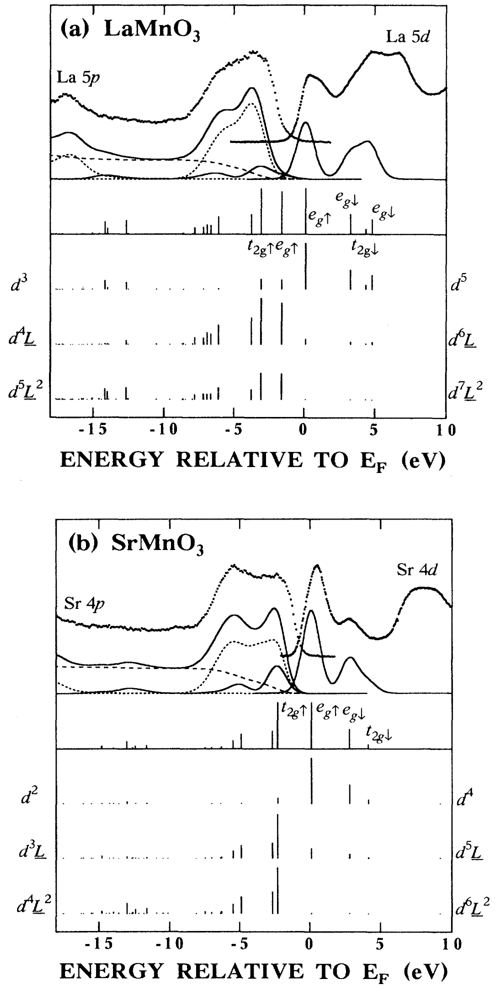

FIG. 4. Cluster-model analyses of the valence-band photoemission and O 1*s* XAS spectra of $LaMnO_3$ (a) and $SrMnO_3/La_{0.1}Sr_{0.9}MnO_3$ (b). Upper panels: Calculated valence-band and O 1*s* XAS spectra (solid lines) are compared with the experimental spectra (dots). The energies of the O 1*s* XAS spectra were referenced to that of the O 1*s* binding energies. The gap between the calculated photoemission and XAS spectra is set equal to the band gap calculated using the cluster model. Lower panels: Decomposition of the calculated spectra into final-state configurations.

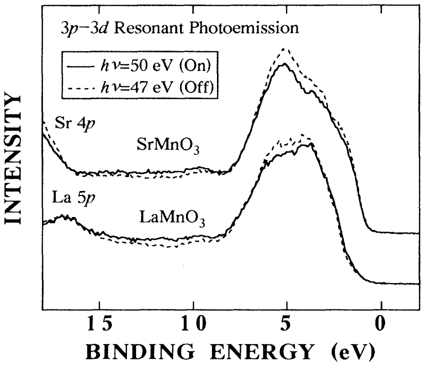

FIG. 5. Mn $3p$-$3d$ resonant photoemission spectra of $LaMnO_3$ and $SrMnO_3$.

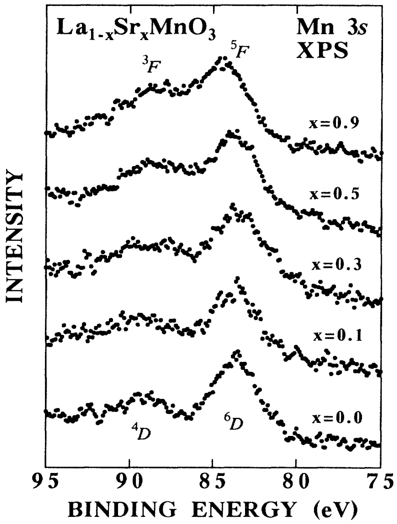

FIG. 6. Mn $3s$ core-level XPS spectra of $La_{1-x}Sr_xMnO_3$ for various compositions.

the $t_{2g\uparrow}$ states. As for the O $1s$ XAS spectrum, the first peak is due to transitions into the $e_{g\uparrow}$ states, and the lower-energy side of the broad second structure is assigned to a superposition of the $e_{g\downarrow}$ states and the $t_{2g\downarrow}$ states, overlapping with the La $5d$ band. These states have relatively pure d^5 character without strong mixture of the $d^6\underline{L}$ configuration.

For the valence-band spectrum of $SrMnO_3$ shown in Fig. 4(b), the main band located at 1–6 eV below the Fermi level will have heavily mixed $d^3\underline{L}$-$d^4\underline{L}^2$ character, while the satellite structure located at 11–15 eV has mainly $d^4\underline{L}^2$ character. The first peak is emission due to the $t_{2g\uparrow}$ states since there are no electrons in the occupied $e_{g\uparrow}$ levels in $SrMnO_3$. For the O $1s$ XAS spectrum, the first and second structures are due to the $e_{g\uparrow}$ and $e_{g\downarrow}$ states, respectively, and the $t_{2g\downarrow}$ states are located on the higher-energy side of the second structure. These states have mostly d^4 character. The present assignment for the O $1s$ XAS spectra differs somewhat from our previous assignment[20] that the first structure was a superposition of the $e_{g\uparrow}$ and $t_{2g\downarrow}$ bands and the second structure was the band of $e_{g\downarrow}$ character.

IV. EFFECTS OF CARRIER DOPING

A. Mn 3s core levels

The $3s$ core level of the $3d$ TM ion is known to exhibit an exchange splitting. The magnitude of the splitting is given by $(2S+1)G^2(3s,3d)/5$, where S is the local $3d$ spin and $G^2(3s,3d)$ is the Slater exchange integral between the $3s$ and the $3d$ electrons.[34] Although such a simple ionic picture is not strictly valid in the present case because of the strong hybridization between the Mn $3d$ and O $2p$ ligand orbitals and charge transfer induced by the core-hole potential,[35] we expect that it is useful for qualitative argument. In Fig. 6, the Mn $3s$ core levels of $La_{1-x}Sr_xMnO_3$ are shown for various values of x. First of all, the magnitude of the splitting is large, consistent with the high-spin configurations. One can see that the exchange splitting monotonically increases with decreasing x. This indicates that the extra electrons (of mixed p-d character) doped into $SrMnO_3$ are ferromagnetically coupled with the high-spin d^3 configuration of the Mn^{4+} ions. Conversely, the extra holes (of predominant p character) doped into $LaMnO_3$ are antiferromagnetically coupled to the high-spin d^4 configuration of the Mn^{3+} ions.

The doped holes in $La_{1-x}Sr_xMnO_3$ are analogous to those in the high-T_c cuprates, where the hole forms a so-called Zhang-Rice singlet[36] through the antiferromagnetic interaction with the Cu $3d^9$ spin. In the case of the cuprates, increased hole concentration leads to the formation of a paramagnetic metal, whereas in $La_{1-x}Sr_xMnO_3$ the itinerant doped holes of p character align the localized Mn spins ferromagnetically as in Zener's s-d model for ferromagnetic metals.[37]

B. Occupied and unoccupied valence states

The XPS and He II UPS spectra of the valence bands of $La_{1-x}Sr_xMnO_3$ are shown in Figs. 7 and 8, respectively. According to the photoionization cross sections,[30] the emission intensity is due mostly to O $2p$ states in the He II spectra, while the Mn $3d$ component amounts to about 30% of the total valence-band intensity in the XPS spectra. The two structures located at 2–4 and ~6 eV are largely due to the O $2p$ band characteristic of perovskite-type oxides.

In Fig. 8, the UPS spectra are normalized so that the integrated intensity of the valence band is roughly proportional to that expected from the photoionization cross sections of the Mn $3d$ and O $2p$ atomic orbitals. The figure shows that in the spectra for $x=0.3$ and 0.6, the steep edge located around 1.0–2.5 eV (denoted edge A) is ~0.4 eV closer to the Fermi level than that for $x=0.0$, and that it is ~0.8 eV closer to the Fermi level in the $x=0.9$ spectrum. On the other hand, the steep edge lo-

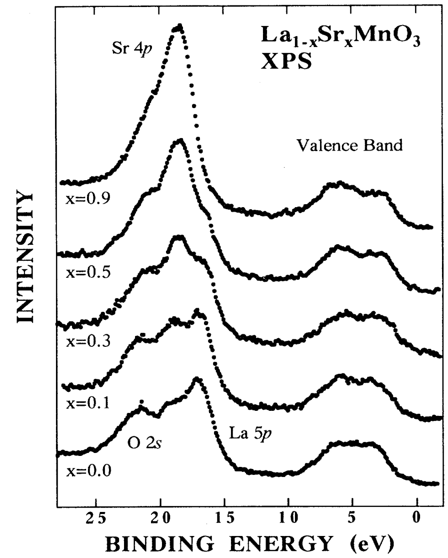

FIG. 7. Valence-band XPS spectra of $La_{1-x}Sr_xMnO_3$ for various compositions.

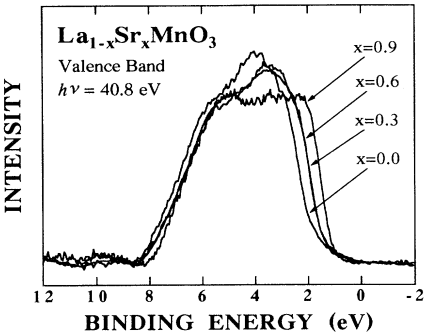

FIG. 9. Valence-band UPS spectra of $La_{1-x}Sr_xMnO_3$ for various compositions, normalized in the same way as in Fig. 8. The backgrounds due to secondary electrons have been subtracted.

cated at 6.5–7.5 eV (denoted edge *B*) shows little shift with *x*. This energy shift is clearly seen in Fig. 9, where the backgrounds due to secondary electrons have been subtracted. This indicates that the valence-band width increases with increasing Sr concentration, possibly because the $GdFeO_3$-type distortion diminishes with *x*. It should be noted that although edge *A* shifts toward the Fermi level in going from $x = 0$ to 0.3, there is no detectable shift within the metallic range, i.e., between $x = 0.3$ and 0.6.

Although edge *A* is shifted toward the Fermi level with *x*, the emission intensity between the Fermi level and ~2 eV below it (denoted tail *C*) decreases with *x*; for $x = 0.9$, the tail almost disappears, see Fig. 10. Therefore, tail *C* (or the shaded region in Fig. 10) is considered to be due to emission from the $e_{g\uparrow}$ band, which accommodates one electron per Mn in $LaMnO_3$ (d^4) and is empty in $SrMnO_3$ (d^3).

The combined UPS and O 1*s* XAS spectra near the Fermi level are displayed in Fig. 11. Here the O 1*s* XAS spectra are normalized at ~20 eV above the Fermi level, where the absorption intensity would be independent of *x*.[20] In order to highlight the changes with composition in the UPS spectra, difference spectra relative to $x = 0.9$ are also shown. To take the difference spectra, the $x = 0.9$ spectrum was shifted so that the two spectra

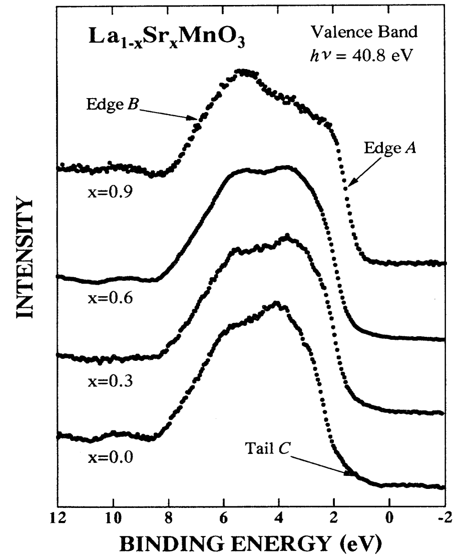

FIG. 8. Valence-band UPS spectra of $La_{1-x}Sr_xMnO_3$ for various compositions. The spectra have been normalized as described in the text.

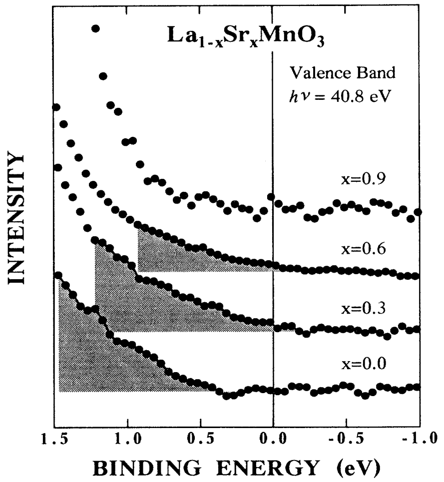

FIG. 10. UPS spectra of $La_{1-x}Sr_xMnO_3$ near the Fermi level on an expanded scale. The shaded region is denoted tail *C* in Fig. 8 and indicates emission from the $e_{g\uparrow}$ band.

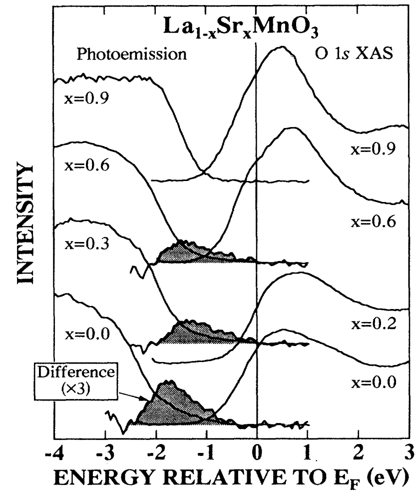

FIG. 11. UPS and O 1*s* XAS spectra near the Fermi level. The O 1*s* XAS spectra are references to the O 1*s* binding energies. The difference spectra relative to $x=0.9$ are also shown. Starting from $SrMnO_3$, the intensity of the $e_{g\uparrow}$ emission in the UPS spectra gradually increases with decreasing x.

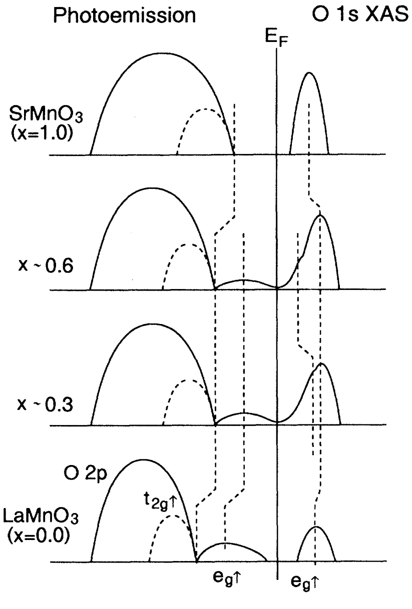

FIG. 12. Schematic picture for the evolution of the electronic structure of $La_{1-x}Sr_xMnO_3$.

align at edge *A*. As the difference spectrum would represent emission of the $e_{g\uparrow}$ electrons, the result shows that the occupied band of $e_{g\uparrow}$ character in $LaMnO_3$ is centered around 1.7 eV below the Fermi level, consistent with the previous result of the spin-polarized photoemission on $La_{1-x}Pb_xMnO_3$.[38] The x dependence of the difference spectra indicates that if we start from $SrMn^{4+}O_3$, which has the high-spin d^3 ($t^3_{2g\uparrow}$) configuration, added electrons occupy the $e_{g\uparrow}$ orbitals and their spectral weight appears within the band gap of $SrMnO_3$. Correspondingly, in the O 1*S* XAS spectra, the intensity of the $e_{g\uparrow}$ band just above the Fermi level decreases with La substitution. (The result is consistent with the recent O 1*s* XAS measurements in the fluorescence yield mode.[39]) We note that the decrease of the intensity of the unoccupied $e_{g\uparrow}$ states is not entirely due to the decrease in the number of unoccupied states but can also be due to the decrease in covalency between Mn and O associated with the increase in Δ_{eff} (see Table I). These behaviors are quite different from what would be expected from a rigid-band model, according to which the Fermi level moves downwards with increasing x within the $e_{g\uparrow}$ band with a fixed line shape: In the rigid-band model, one would expect to observe a sharp Fermi cutoff with high spectral intensity at intermediate x's. A schematic picture of the spectral weight distribution and its evolution with x deduced from the present results is shown in Fig. 12. The present results resemble those of $La_xSr_{1-x}TiO_3$,[5] in which additional spectral weight induced by La substitution (electron doping) appears below the Fermi level within the band gap of $SrTiO_3$ and the peak position of this spectral weight is as deep as ~ 1.5 eV below the Fermi level.

In analogy with the O 1*s* XAS spectra of high-T_c cuprates, one would expect that, in the unoccupied states of the hole-doped $LaMnO_3$, $e_{g\uparrow}$-like spectral weight will appear within the band gap of $LaMnO_3$. Indeed, in the O 1*s* XAS spectra of $La_{1-x}Sr_xFeO_3$ additional spectral weight appears in the band gap of $LaFeO_3$ upon Sr doping.[20] In the O 1*s* XAS spectra of $La_{1-x}Sr_xMnO_3$, however, no such features are observed. Presumably, the spectral weight induced by hole doping overlaps the original $d^4 \rightarrow d^5$ spectral weight (i.e., the upper Hubbard band) of $LaMnO_3$ because of the small band gap of $LaMnO_3$ and/or because of the wide energy distribution of the doping-induced spectral weight.

If we consider the Mn 3*d*–O 2*p* hybridized states near the Fermi level and the band gap as effective *d* states and effective *U*, respectively, the electronic structure near the Fermi level of $La_{1-x}Sr_xMnO_3$ is similar to that of the Hubbard model and therefore can be mapped onto an effective Hubbard model with orbital degeneracy. In the composition range of ferromagnetic metals at low temperatures, the e_g band is fully polarized due to Hund's rule coupling with the fully polarized $t_{2g\uparrow}$ bands, so that a spinless model becomes relevant for the $e_{g\uparrow}$ electrons. The $e_{g\uparrow}$ electrons can then be treated in a modified single-band Hubbard model, where the spin degrees of freedom are replaced by the orbital degrees of freedom (x^3-y^2 and $3z^2$-r^2) of the $e_{g\uparrow}$ subband. Spin fluctuations in the single-band Hubbard model may then be replaced by fluctuations of the electric quadrupole moment of the degenerate $e_{g\uparrow}$ orbitals, which will be coupled with lattice distortion. Magnetic ordering in the standard Hubbard model would correspond to the formation of an orbital superlattice in the present case. Theoretical studies of Mn oxides from this point of view, and their comparison with Cu oxides (modeled by a nondegenerate Hubbard model) and Ti oxides (modeled by a degenerate Hubbard model) would be of great interest.

C. Fermi-level shift with carrier doping

In Fig. 13, the energies of several core levels and valence-band features are plotted as functions of Sr concentration. The figure shows that the relative binding energies of all the core levels decrease with x in going from the semiconducting phase ($x \leq 0.1$) to the metallic phase ($x \gtrsim 0.3$), implying that the Fermi level is lowered with hole doping. (The absolute binding energies of the core levels are listed in Table III.)

TABLE III. Core-level binding energies for $La_{1-x}Sr_xMnO_3$ (in eV). For the La $3d_{5/2}$ peaks, the lower binding-energy peaks are listed. Errors are ± 0.3 eV for the Mn 3s peaks, and ± 0.1 eV otherwise.

x	0.0	0.1	0.3	0.5	0.9
O 1s	529.7	529.6	529.3	529.3	529.4
Mn $2p_{3/2}$	641.9	641.8	641.6	641.8	642.3
Mn 3s	83.5		87.7	83.8	84.3
Mn 3p	49.0	49.0	48.9	49.2	49.8
La $3d_{5/2}$	834.2	834.2	833.7	833.7	
Sr $3d_{3/2}$		132.8	132.4	132.3	132.4

For higher Sr concentration $x > 0.2$, the energy shifts of the various spectral features become rather complicated. The Mn 2p core level is shifted back toward higher binding energy in going from the metallic phase ($0.3 \leq x \leq 0.6$) to the Sr-rich semiconducting phase ($x \geq 0.8$). This can be simply attributed to an ordinary chemical shift arising from the increase of the Mn valence. On the other hand, the O 1s core level is shifted back only slightly and the La 3d and Sr 3d levels are not shifted back appreciably. Since the A-site ions are not involved in the chemical bonding or the metallic conductivity, the shifts of the La and Sr core levels would rather faithfully reflect the shift of the Fermi level if the changes in the Madelung potential with x are negligibly small. Since the change in the Madelung potential would lower the Sr core level with x, the almost constant Sr core-level binding energy implies that the changes in the Madelung potential are almost completely screened and that the La and Sr core-level shifts reflect the real Fermi-level shift. The shift of edge A, which consists of the 3d $t_{2g\uparrow}$ and O 2p states, as well as the shift of the top of the $e_{g\uparrow}$ band, are parallel to those of the Sr 3d and O 1s core levels up to $x = 0.6$, giving further support to the downward Fermi-level shift at $x \leq 0.6$. However, it should be noted that the shifts of the La and Sr core levels are not detectable within the metallic phase, indicating that the Fermi-level shift is in fact very small within the metallic phase ($0.3 \leq x \leq 0.6$).

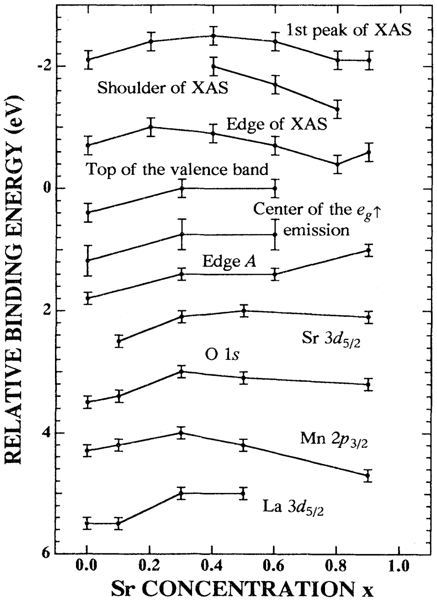

FIG. 13. Energy shifts of core and valence levels in $La_{1-x}Sr_xMnO_3$ as functions of Sr concentration x. Note that the figure shows the energy shifts as a function of x for each level, and not the absolute binding energies.

The features in the O 1s XAS spectra are also shifted back toward lower energies in going from the metallic phase to Sr-rich semiconducting phase like the Mn 2p core level. This can be understood from the predominance of Mn 3d character in the unoccupied states. At $x \geq 0.6$, only edge A shows a further shift, unlike the other levels, which we attribute to the broadening of the O 2p band.

V. CONCLUSION

We have studied the electronic structure of $La_{1-x}Sr_xMnO_3$ by photoemission spectroscopy, O 1s x-ray-absorption spectroscopy, and subsequent cluster-model analyses. The ground state of $LaMnO_3$ is found to consist of $\sim$50% d^4, $\sim$40% $d^5\underline{L}$, and $\sim$10% $d^6\underline{L}^2$ states, and that of $SrMnO_3$ of $\sim$40% d^3, $\sim$50% $d^4\underline{L}$, and $\sim$10% $d^5\underline{L}^2$ states. The two end members are charge-transfer insulators, but the band gap of $SrMnO_3$ also has considerable p-p character. The double-exchange mechanism in the metallic phase is caused by the itinerant holes doped into $LaMnO_3$ of mainly oxygen p character with $e_{g\uparrow}$ symmetry: These holes are antiferromagnetically coupled with the d^4 local moments of the Mn^{3+} ions, and align them ferromagnetically. The hole carriers in the relatively wide $e_{g\uparrow}$-symmetry band are responsible for the metallic conductivity and both the e_g electrons and the relatively well localized Mn t_{2g} electrons are responsible for the ferromagnetism.

The changes in the electronic structure near the Fermi level with carrier doping are not rigid-band-like: Starting from $SrMnO_3$, so-called in-gap spectral weight appears in the valence-band photoemission spectra well (1–2 eV) below the Fermi level and grows in intensity with electron doping. The photoemission intensity at the Fermi level remains low even in the metallic phase. The origin of this non-rigid-band behavior as a function of carrier doping remains unclear at present. We point out the importance of the orbital degeneracy of the $e_{g\uparrow}$ band and the possibility of orbital fluctuations in the ferromagnetic phase.

ACKNOWLEDGMENTS

We would like to thank the staff of Synchrotron Radiation Laboratory for valuable technical support. All the calculations have been performed using a VAX/VMS system at the Meson Science Laboratory, Faculty of Science, University of Tokyo. Useful discussions with Professor D. D. Sarma, Professor Y. Tokura, and Dr. P. Steiner are gratefully acknowledged. The present work is supported by a Grant-in-Aid for Scientific Research from the Ministry of Education, Science and Culture, Japan. One of us (T.S.) is supported by a Fellowship of the Japan Society for the promotion of Science for Japanese Junior Scientists.

---

*Present address: Department of Materials Science, Faculty of Science, Hiroshima University, Higashi-Hiroshima 724, Japan.

[1] J. G. Bednorz and K. A. Müller, Z. Phys. B **64**, 189 (1986).

[2] A. Fujimori and F. Minami, Phys. Rev. B **30**, 957 (1984).

[3] J. Zaanen, G. A. Sawatzky, and J. W. Allen, Phys. Rev. Lett. **55**, 418 (1985); S. Hüfner, Z. Phys. B **61**, 135 (1985); J. Zaanen and G. A. Sawatzky, Can. J. Phys. **65**, 1262 (1987); H. Eskes, L. H. Tjeng, and G. A. Sawatzky, Phys. Rev. B **41**, 288 (1990); J. Ghijsen, L. H. Tjeng, H. Eskes, G. A. Sawatzky, and R. L. Johnson, *ibid.* **42**, 2268 (1990); A. Fujimori, N. Kimizuka, T. Akahane, T. Chiba, S. Kimura, F. Minami, K. Siratori, M. Taniguchi, S. Ogawa, and S. Suga, *ibid.* **42**, 7580 (1990).

[4] H. Eisaki, S. Uchida, T. Mizokawa, H. Namatame, A. Fujimori, J. van Elp, P. Kuiper, G. A. Sawatzky, S. Hosoya, and H. Katayama-Yoshida, Phys. Rev. B **45**, 12 513 (1992).

[5] A. Fujimori, I. Hase, M. Nakamura, H. Namatame, Y. Fujishima, Y. Tokura, M. Abbate, F. M. F. de Groot, M. T. Czyzyk, J. C. Fuggle, O. Strebel, F. Lopez, M. Domke, and G. Kaindl, Phys. Rev. B **46**, 9841 (1992).

[6] A recent work suggests that some Ti and V oxides may be charge-transfer insulators [T. Uozumi, K. Okada, and A. Kotani, J. Phys. Soc. Jpn. **62**, 2595 (1993)].

[7] G. H. Jonker and J. van Santen, Physica **16**, 337 (1950).

[8] J. H. van Santen and G. H. Jonker, Physica **16**, 599 (1950).

[9] H. L. Yakel, Acta Crystallogr. **8**, 394 (1955).

[10] E. O. Wollan and W. C. Koehler, Phys. Rev. **100**, 545 (1955).

[11] W. C. Koehler and E. O. Wollan, J. Phys. Chem. Solids **2**, 100 (1957).

[12] G. Matsumoto, J. Phys. Soc. Jpn. **29**, 606 (1970).

[13] A. Chainani, M. Mathew, and D. D. Sarama, Phys. Rev. B **47**, 15 397 (1993).

[14] T. Takeda (unpublished).

[15] T. Takeda and S. Ohara, J. Phys. Soc. Jpn. **37**, 275 (1974).

[16] G. H. Jonker, Physica **20**, 1118 (1954).

[17] C. Zener, Phys. Rev. **82**, 403 (1951).

[18] P.-G. de Gennes, Phys. Rev. **118**, 141 (1960).

[19] R. von Helmolt, J. Wecker, B. Holzapfel, L. Schultz, and K. Samwer, Phys. Rev. Lett. **71**, 2331 (1993); Y. Tokura, A. Urushibara, Y. Moritomo, T. Arima, A. Asamitsu, G. Kido, and N. Furukawa, J. Phys. Soc. Jpn. **63**, 3931 (1994).

[20] M. Abbate, F. M. F. de Groot, J. C. Fuggle, A. Fujimori, O. Strebel, F. Lopez, M. Domke, G. Kaindl, G. A. Sawatzky, M. Takano, Y. Takeda, H. Eisaki, and S. Uchida, Phys. Rev. B **46**, 4511 (1992).

[21] A. E. Bocquet, T. Mizokawa, T. Saitoh, H. Namatame, and A. Fujimori, Phys. Rev. B **46**, 3771 (1992).

[22] A. E. Bocquet, T. Saitoh, T. Mizokawa, and A. Fujimori, Solid State Commun. **83**, 11 (1992); A. Fujimori, A. E. Bocquet, T. Saitoh, and T. Mizokawa, J. Electron Spectrosc. Relat. Phenom. **62**, 141 (1992).

[23] J. Park, S. Ryu, M. Han, and S.-J. Oh, Phys. Rev. B **37**, 10 867 (1988); S.-J. Oh, G.-H. Gweon, and J.-G. Park, Phys. Rev. Lett. **68**, 2850 (1992).

[24] J. Kanamori, Prog. Theor. Phys. **30**, 275 (1963); B. H. Brandow, Adv. Phys. **26**, 651 (1977).

[25] S. Sugano, Y. Tanabe, and H. Kamimura, *Multiplets of Transition-Metal Ions in Crystals* (Academic, New York, 1970).

[26] Y. Tanabe and S. Sugano, J. Phys. Soc. Jpn. **9**, 766 (1954).

[27] D. J. Lam and B. W. Veal, Phys. Rev. B **22**, 5730 (1980).

[28] The Lorentzian full width at half maximum (FWHM) is taken to be $2\Gamma_n = 2\Gamma_0 + \alpha\Delta E$, where $2\Gamma_0 = 2.0$ eV is the Lorentzian FWHM of the main peak, ΔE is the energy separation from the main peak, and α is a constant (~ 0.01). A Gaussian broadening of about 1.6 eV FWHM is also applied.

[29] T. Mizokawa, H. Namatame, A. Fujimori, K. Akeyama, H. Kondoh, H. Kuroda, and N. Kosugi, Phys. Rev. Lett. **67**, 1638 (1991).

[30] J. J. Yeh and I. Lindau, At. Data Nucl. Data Tables **32**, 1 (1985). At $h\nu \sim 100$ eV, the Mn $3d$ to O $2p$ relative cross section ($\sim 17\%$) is larger than that ($\sim 7\%$) for $h\nu \sim 40$ eV or that ($\sim 3\%$) for $h\nu \sim 20$ eV but is still much smaller than unity. Therefore, the spectra in Fig. 4 are still dominated by emission from O $2p$ states.

[31] This empirical factor has been successfully used in previous studies on TM oxides (Refs. 2–4).

[32] The Lorentzian FWHM of the first peaks of the valence-band and O $1s$ XAS spectra was fixed to be ~ 0 eV, and the proportional coefficient for the additional broadening $\alpha = 0.001$–0.005 was assumed. The Gaussian FWHM was taken to be ~ 1.6 eV.

[33] Due to the O $1s$ core-hole potential, the XAS spectra may be distorted from the line shape of the unoccupied density of states. Such an effect is not well understood at present, but will not affect the qualitative features of the spectra and their changes with x as discussed in the present paper.

[34] A. E. Bocquet, A. Fujimori, T. Mizokawa, T. Saitoh, H. Namatame, S. Suga, N. Kimizuka, Y. Takeda, and M. Takano, Phys. Rev. B **45**, 1561 (1992).

[35] K. Okada, A. Kotani, and T. Thole, J. Electron Spectrosc. Relat. Phenom. **58**, 325 (1992).

[36] F. C. Zhang and T. M. Rice, Phys. Rev. B **37**, 3759 (1988).

[37] C. Zener, Phys. Rev. **81**, 440 (1951).

[38] S. F. Alvarado, W. Eib, P. Munz, H. C. Siegmann, M. Campagna, and J. P. Remeika, Phys. Rev. B **13**, 4918 (1976).

[39] D. D. Sarma, O. Rader, T. Kachel, A. Chainani, M. Mathew, K. Holldack, W. Gudat, and W. Eberhardt, Phys. Rev. B **49**, 14 238 (1994).